Self-supervised Spatial-Temporal Learner for Precipitation Nowcasting

Haotian Li[†], Arno Siebes, Siamak Mehrkanoon

Department of Information and Computing Science, Utrecht University, Utrecht, The Netherlands

{h.li2, a.p.j.m.siebes, s.mehrkanoon}@uu.nl

Abstract—Nowcasting, the short-term prediction of weather, is essential for making timely and weather-dependent decisions. Specifically, precipitation nowcasting aims to predict precipitation at a local level within a 6-hour time frame. This task can be framed as a spatial-temporal sequence forecasting problem, where deep learning methods have been particularly effective. However, despite advancements in self-supervised learning, most successful methods for nowcasting remain fully supervised. Selfsupervised learning is advantageous for pretraining models to learn representations without requiring extensive labeled data. In this work, we leverage the benefits of self-supervised learning and integrate it with spatial-temporal learning to develop a novel model, SpaT-SparK. SpaT-SparK comprises a CNN-based encoder-decoder structure pretrained with a masked image modeling (MIM) task and a translation network that captures temporal relationships among past and future precipitation maps in downstream tasks. We conducted experiments on the NL-50 dataset to evaluate the performance of SpaT-SparK. The results demonstrate that SpaT-SparK outperforms existing baseline supervised models, such as SmaAt-UNet, providing more accurate nowcasting predictions.

Index Terms—Self-supervised learning, Precipitation nowcasting, Spatial-temporal learning

I. INTRODUCTION

Nowcasting is the short-term prediction of weather and is crucial for weather-dependent decision-making. The World Meteorological Organization defines nowcasting as forecasting with local detail, by any method, over a period from the present to six hours ahead, including a detailed description of the present weather [1]. Nowcasting plays a crucial role in weather-dependent activities, for instance: (1) accurate nowcasting addresses the challenge of flood prevention posed by sudden precipitation or extremes [2]; (2) it allows water resource management to optimize reservoir levels, plan irrigation schedules, and prevent shortages [3]; (3) nowcasting informs cities' decisions in managing stormwater drainage systems, prevent urban flooding, and ensure the safety of residents [4].

Given the cruciality of nowcasting, numerical weather prediction (NWP) models have been developed [5] to forecast the weather. NWP models are meteorology-theory-guided mathematical models for weather forecasting and, as a result, involve complex equations representing the dynamics and thermodynamics of the atmosphere [6]. However, NWP models pose challenges in nowcasting tasks. Solving such equations is non-trivial and time-consuming, leading to the delayed outcomes

of NWP models [7]. Therefore, NWP models struggle to meet the "short-time ahead" requirement for nowcasting.

Machine learning and deep learning models are promising candidates for nowcasting/forecasting applications [8]–[13]. Extensively trained, these models achieve fast inference. In addition, the development of these models benefits from the increasing availability of radar image data, due to advances in remote sensing techniques. Trained with the precipitation data, CNN-based models [9], [10] demonstrated accurate performances. Precipitation nowcasting problem can be formulated as a spatial-temporal sequence problem as well, both the input and prediction target are spatial-temporal sequences [8].

Self-supervised learning (SSL) is a label-free learning paradigm. In SSL, the model is trained on pretext tasks using the data itself to generate supervisory signals, rather than relying on external labels provided by humans. SSL has shown its power in learning representations in various application domains such as computer vision [14], biomedical signal analysis [15], [16], natural language processing [17] among others. SSL improves model accuracy, robustness, and uncertainty [18], [19]. [20] pioneered masked image modeling (MIM), which masks part of an image and reconstructs it to minimize error. MIM is widely used in SSL for learning image representations in various tasks [21]–[23].

Since SSL is proved to be beneficial to learning representations, we design a self-supervised learning pipeline to help the model extract meaningful representations from the precipitation map data and boost the performance of precipitation nowcasting. With the success of enabling SSL on CNNs with SparK [24], we propose the *Spatial-Temporal SparK* model (termed as SpaT-SparK) for precipitation nowcasting. In summary, the contribution of this work is two-fold:

- Providing a simple self-supervised spatial-temporal learning model, SpaT-SparK, for precipitation nowcasting task.
- Validating the effect of proposed SpaT-SparK on the precipitation data in the Netherlands.

The SpaT-SparK model comprises two parts to perform the precipitation nowcasting task: (1) an encoder-decoder structure, which is pretrained with the MIM task, learning to encode and decode the representation of input precipitation maps; (2) a translation network to capture temporal relationships between the representation of the past and that of the future precipitation maps. In the self-supervised pretraining MIM task, the encoder learns how to encode a sequence of

[†] Corresponding author

precipitation maps to the latent representation, and the decoder learns how to reconstruct the original maps. Subsequently, the translation network learns to capture the temporal dependency between representations of past and future precipitation maps in downstream tasks. The code is available at https://github.com/htlee6/SpaT-SparK

II. RELATED WORK

Deep Learning for Precipitation Nowcasting: Deep learning is deployed to tackle precipitation nowcasting tasks. ConvLSTM [8] leveraged the temporal dependency among each image input dynamically and improved the performance by extending fully connected LSTM to convolutional structures. [9] used UNet [25], a 2D convolutional encoder-decoder architecture, to capture the structural difference between different image inputs to make predictions. SmaAt-UNet [10], AA-TransUNet [26], SAR-UNet [27] and Broad-UNet [28] further developed variations of UNet tailored for nowcasting tasks. SmaAt-UNet reduced parameter size and achieved comparable performance in precipitation nowcasting by introducing depthwise separable convolutions (DSC) [29] and CBAM [30] in UNet structures. AA-TransUNet and SAR-UNet further improved performance using the TranUNet backbone and residual DSC blocks, respectively. The Broad-UNet, with asymmetric parallel convolutions and an ASPP module, captures complex patterns with fewer parameters than UNet. Beyond deterministic models, [11] employed generative probabilistic models for reliable predictions, while [31] introduced GA-SmaAt-GNet, a generative adversarial framework for extreme precipitation nowcasting. [32] framed the task as spatialtemporal graph sequence nowcasting. Large-scale models were developed in the weather forecasting/nowcasting task. Graph-Cast [33], Pangu-Weather [34], FourCastNet [35] were large deep learning models trained on large scale data and achieving optimal performances.

Self-supervised Learning: SSL is a promising way to signal supervisory by designing pretext tasks. SSL is categorized as contrastive, generative, and contrastive-generative [36], [37]. There are masked language modeling (MLM) and masked image modeling (MIM) for learning representations in language and image tasks respectively. As an instance of MLM, BERT [38] uses a unique [MASK] token at random positions to enable self-supervised pretraining on large-scale unlabeled corpora. Successive works, e.g. RoBERTa [39] were built upon the findings of BERT. Masked auto-encoder (MAE) [21] extended the idea of MLM from natural language to computer vision and learned featured latent representations from image data with a ViT-based [40] encoder and decoder. Motivated by MAE, Man et al. proposed W-MAE [41], which utilizes MAE in multi-variable weather forecasting and precipitation forecasting tasks on a 6-hour basis (ERA5 [42] dataset). SparK [24] breaks through the limitation of specific ViTbased encoder-decoders, and generalize MIM to CNN-based encoders-decoders with the successfully verified benefits of hierarchical features in vision tasks. SimVP v2 [43] reveals the relations and differences between self-supervised learning and spatial-temporal predictive learning, and provides a recurrent-free model example [44]. Despite these developments, the performance of self-supervised weather forecasting model, such as W-MAE, is tested on long-interval dataset. A self-supervised nowcasting model is necessary for the prediction in the near future. In this work, we introduce SpaT-SparK, a self-supervised spatial-temporal learning model motivated by SparK and SimVP v2, to tackle the short-time lead precipitation nowcasting problem on the Netherlands precipitation dataset.

III. APPROACH

The model schematic is shown in Fig.1. There are 3 main components in this model: an encoder, a decoder, and a translation network. In pretraining, the encoder and the decoder are trained with masked image reconstruction task. The input images are patchified and masked before they are passed to the encoder. Tube masking [45] is adopted as the masking strategy in the pipeline to help the model capture useful spatial-temporal structures. The encoder learns how to represent the sequence of input masked precipitation maps in the latent space, while the decoder learns how to reconstruct the images given the latent representation. Translation network is not involved in the pretraining. In fine-tuning, the learning objective is to predict future precipitation maps given the past ones. The translation network aims to translate the latent representation of the past images generated by the encoder to that of the future images, so that the pretrained decoder can reconstruct the images given the correct latent representation.

Hierarchical Encoder and Decoder We use SparK [24], the self-supervised learning convolutional encoder-decoder model, as the foundation. SparK built the encoder and the decoder in a hierarchical fashion as UNet [25].

The encoder is composed of sparse convolution layers, and it downsamples the input images and generates multi-scale feature maps of different resolutions. We choose ResNet-18 [46] (Fig.1b, left side) as the encoder unless further specified. Given an image with height H and width W, the encoder generates sparse feature maps $\mathbf{S} = \{S_i \mid i=1...4\}$ at 4 scales with resolutions of $\frac{H}{4} \times \frac{W}{4}$, $\frac{H}{8} \times \frac{W}{8}$, $\frac{H}{16} \times \frac{W}{16}$, and $\frac{H}{32} \times \frac{W}{32}$ respectively. Since the feature maps generated by the encoder are sparse, a densify network is necessary to fill in the empty positions of sparse feature maps with mask embedding $[M_i]$ at the i-th level as follows:

$$S_i' = S_i + [M_i],$$

where $[M_i]$ is a learnable 2D map parameter, initialized with truncated normal distribution as in SparK, and S_i' is the dense feature map at the *i*-th level. The decoder network decodes the dense feature maps and then reconstructs the original images. We use the same LightDecoder as in SparK. The LightDecoder consists of 3 successive UNet blocks (Fig.1b, right side), $\{B_1, B_2, B_3\}$ with different hyperparameters, to upsample and decode features from corresponding levels and a Conv2D layer for final projection.

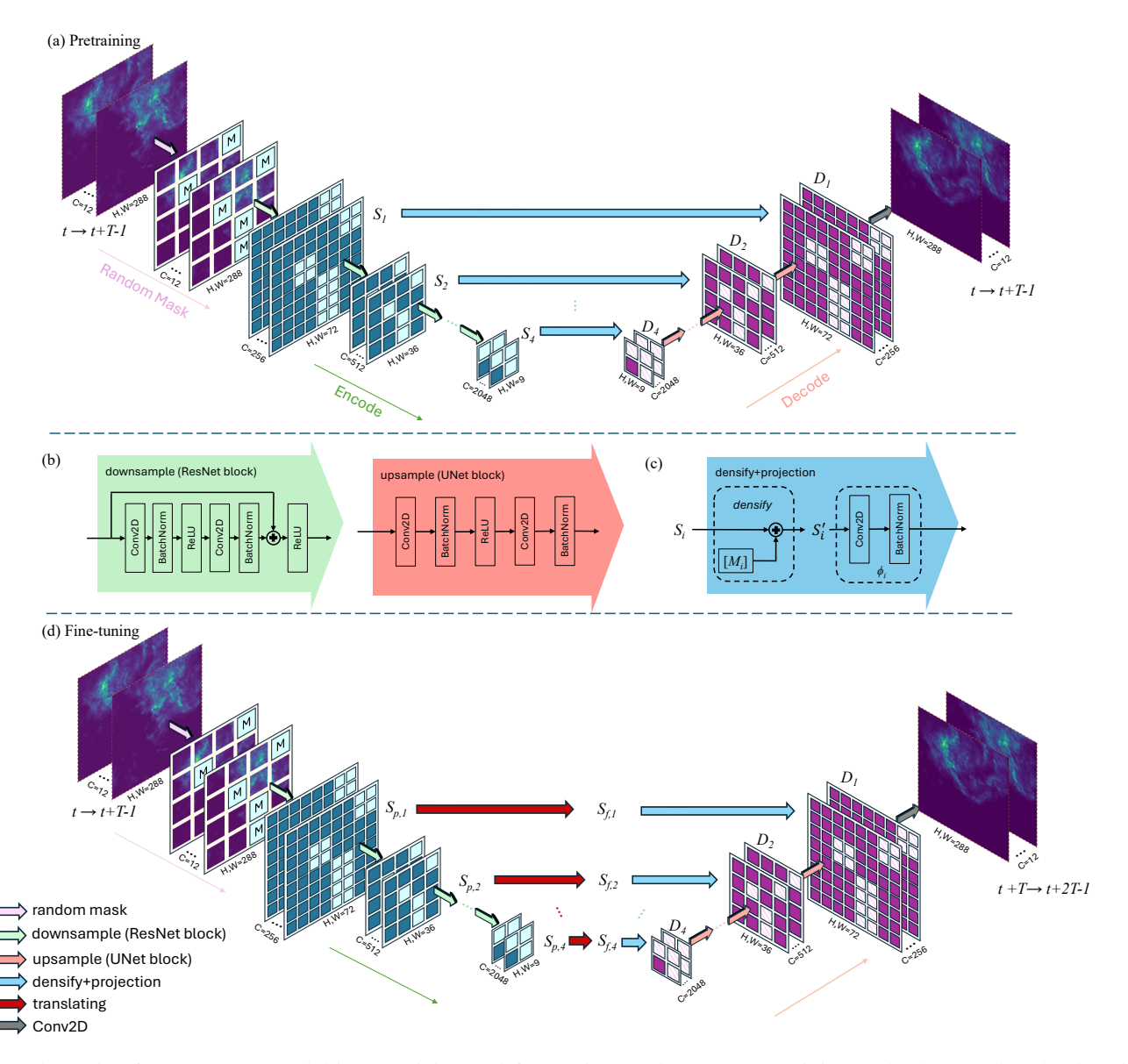


Fig. 1: Schematic of SpaT-SparK model in pretraining and fine-tuning mode. (a) In pretraining, only the encoder, the decoder, and the densifying network are pretrained. (b) Architecture of encoder (ResNet) blocks and decoder (UNet) blocks. (c) Illustration of densify network and successive projection. (d) In fine-tuning, the encoder, the decoder, and the densifying network are initialized with pretrained weight, and the translation network is trained from scratch. The 4th hierarchy is adapted for better visualization purpose; the visualizations of the outputs in (a) and (d) are adapted for illustration purposes, and do not reflect the actual predictions.

Denoting the set of decoded feature maps as $\mathbf{D} = \{D_i \mid i = 1...4\}$ and the set of projection layers $\phi = \{\phi_i \mid i = 1...4\}$ for 4 levels, composed of normalization layers and Conv2D layers. D_4 is then projected by projection layer ϕ_4 :

$$D_4 = \phi_4(S_4'),$$

for $\{D_i \mid i=3...1\}$, the decoded feature map is derived from that of the lower level D_{i+1} and the dense feature map at the same level S_i' . S_i' is projected to comply with the decoded feature map dimension with the projection layer ϕ_i at the i-th

layer:

$$D_i = B_i(D_{i+1}) + \phi_i(S_i'), i = 3...1.$$

At last, the output prediction \hat{X} is derived from the final projection on D_1 as follows:

$$\hat{X} = \text{Conv2D}(D_1),$$

where \hat{X} is the output prediction of precipitation maps depending on the learning objective in pretraining or fine-tuning phase.

Translation Network We use a translation network to ease the task of the encoder and the decoder in fine-tuning. In the MIM pretraining, the encoder and decoder can collaborate well with each other to represent the input sequence in latent space and then reconstruct it. However, in the fine-tuning, it is difficult for the encoder and the decoder to shift from the learned knowledge since they were well-trained on the reconstruction task. The translation network can manage to learn the shift between the past and future representations, so that the well-trained encoder and decoder can fully use their abilities of extracting and reconstructing from representations learned in pretraining. The joining of translation network reliefs the difficulty of fine-tuning the parameters of encoder and decoder compared to the approaches without translation network, e.g. SparK. The encoder, the translation network, and the decoder are the main components of SpaT-SparK. The three components collaborate to make accurate predictions.

The translation network maps the latent representation of the past image sequence at the i-th level $S_{p,i}$ to that of the corresponding future image sequence $S_{f,i}$. \mathbf{S}_p and \mathbf{S}_f are the sets of features of past and predicted future precipitation maps obtained at different levels of the network respectively. Since the features are 2-dimensional, the translation network are expected to take the 2D features as input and then output 2D features. To simplify, we select the combination of a Conv2D layer and tanh layer as non-linear layer for features at 4 levels. We refer translation network as Θ , and the sublayer at the i-th layer as θ_i :

$$\theta_i(\cdot) = \tanh(\text{Conv2D}(\cdot)),$$

$$\mathbf{S}_f = \Theta(\mathbf{S}_p) = \{ S_{f,i} \mid S_{f,i} = \theta_i(S_{p,i}), i = 1...4 \}.$$

Pretraining and Fine-tuning In pretraining, the objective of SpaT-SparK is to reconstruct the precipitation map sequence of length T. SpaT-SparK model leverage the advantages of learning hierarchical and sparse feature representation in SparK. The optimization goal is to minimize the per-patch normalized L2 error between the prediction and the ground truth precipitation maps on masked patches only. The pretraining can be abstracted from a high level as:

$$\underset{\mathbf{W}}{\operatorname{arg\,min}}\ \operatorname{loss}(X_{t\to t+T-1}*mask, \hat{X}_{t\to t+T-1}*mask),$$

where

$$\hat{X}_{t \to t+T-1} = \text{DEC}(\text{Densify}(\text{ENC}(X_{t \to t+T-1}))).$$

W refers to the weights of encoder, decoder and densify network in SpaT-SparK model, $\hat{X}_{t \to t+T-1}$ is the reconstruction of the precipitation map sequence from time t to t+T-1 while $X_{t \to t+T-1}$ is the input precipitation map sequence from time t to t+T-1.

In fine-tuning, the objective of SpaT-SparK is to translate the precipitation map sequence in the past to that in the future. The pretrained components of SpaT-SparK model performs the major task of encoding and decoding the past and future precipitation maps, and help to train the translation network

from scratch. The fine-tuning can be abstracted from a high level as:

$$\underset{\mathbf{W},\mathbf{W}_{T}}{\operatorname{arg \, min}} \ \operatorname{loss}(X_{t+T\to t+2T-1},\hat{X}_{t+T\to t+2T-1}),$$

where

$$\hat{X}_{t+T \to t+2T-1} = \\ \text{DEC}(\text{Densify}(\text{Translate}(\text{ENC}(X_{t \to t+T-1})))).$$

 \mathbf{W}_T refers to the weight of the translation network of SpaT-SparK model.

IV. NL-50 DATASET

The NL-50 dataset [10] is a precipitation map dataset within the range of the Netherlands and its surroundings from 2016-2019, measured by Royal Netherlands Meteorological Institute¹ (KNMI, Koninklijk Nederlands Meteorologisch Instituut). The data is measured by both radars in De Bilt (52.1017 N, 5.1783 E) and Den Helder (52.9533 N, 4.7900 E). We followed the same data preprocessing steps as in [10] and also use min-max scaled dataset. Similar to [10], we filter the data where the number of above-threshold pixels are greater than certain values. We set the threshold to 0.5mm/h, and select the map images where the number of above-threshold pixels greater than 50% of single the pixels. We define the length of input image sequences for SpaT-SparK model as T. Then we combine the first T maps with subsequent T maps to make sequences: the first T maps are used as input images for both MIM pretraining and fine-tuning, and the last T maps are used as prediction target for fine-tuning. In this work, T images are converted to a sequence, therefore the input and the output both have the shape of [T, H, W]. The dataset is partitioned to training (2016-2018) and testing sets (2019) by year. The training set has 5734 datapoints while the testing set has 1557 datapoints.

V. NL-50 EXPERIMENT

A. Experiment Settings

We choose different experiment settings for pretraining and fine-tuning phases. We use sequences length T=12 in both pretraining and fine-tuning. In pretraining, we choose batch size 256, base learning rate 2×10^{-4} with linear learning rate annealing scheduler, training epoch 1400, warm-up epoch 40, mask ratio 0.6 as the hyperparameters, and LAMB optimizer [47] with weight decay 0.04 to update the weights. The optimization objective is to minimize the per-patch normalized L2 error on the masked patches. This has been proven to enable the model to learning more informative features from data [21], [24]. In the fine-tuning, we choose batch size 196, base learning rate 1.5×10^{-4} , training epoch 200, warm-up epoch 40, mask ratio 0.6 as the hyperparameters, and LAMB optimizer with weight decay 0.05 to update the weights. The optimization objective is to minimize the L2 error on both masked and unmasked patches.

¹https://dataplatform.knmi.nl/

B. Metrics

We evaluate the model performances with multiple metrics. To calculate the metrics, the raw output and the model prediction are reverted with inverse min-max scaling (unit: mm/5min). The ground truth and prediction maps are thresholded with 0.5mm/h, and pixel-wise positive and negative masks are created. Given those, we compute the confusion matrix and mark true positive (TP), false positive (FP), false negative (FN), and true negative (TN) pixels. Similar to [10], we use pixel-wise MSE (pMSE, eq.1, X, X are predictions and ground truth respectively), accuracy, precision, recall, F1 score, critical success index (CSI, eq.2), false alarm rate (FAR, eq.3), and Heidke skill score (HSS, eq.4) to evaluate the performance of the evaluated models.

$$pMSE = \frac{\|X - \hat{X}\|_2^2}{H \times W},$$

$$CSI = \frac{TP}{TP + FP + FN},$$
(2)

$$CSI = \frac{TP}{TP + FP + FN},$$
(2)

$$FAR = \frac{FP}{TP + FP},\tag{3}$$

$$HSS = \frac{TP \times TN - FP \times FN}{(TP + FN)(FN + TN) + (TP + FP)(FP + TN)}.$$
(4

C. Results

Overall Performance We compared the performances of SpaT-SparK and the baseline models, i.e. SmaAt-UNet and SparK with ResNet-18 or ResNet-50 as the encoder, in Table I. The results showed that SpaT-SparK with ResNet-18 as the encoder has the lowest pMSE. Comparing to SmaAt-UNet, the pMSE decreased by 8.9%. Comparing to SparK, the pMSE decreased in either encoder (-1×10^{-4}) and -7×10^{-4} for ResNet-50 and ResNet-18, respectively). This decrease indicates that the translation network is an effective component to perform the temporal transformation. With the collaboration between the translation network and the encoder and decoder, the learning task of the encoder and decoder is less difficult than that in SparK model. Notably, SpaT-SparK achieves the highest accuracy among all the models, outperforming the baseline SmaAt-UNet model by large margins (18%). The precision metric of the SpaT-SparK model improved by 7.4%, and FAR improved by 12.8%. However, there are drops in recall, F1, CSI, and HSS. The results shine some light on that SSL can make convolutional networks more powerful in precipitation nowcasting.

Performance on Single Time Step We evaluated the model performance on each single time step to investigate the reliability of model with different time offsets. The metrics used for overall performance elevation are also used for evaluations on each single time step. The time offset is referred as t, where t=1 indicates the first prediction map. The results are shown in Fig.2. In Fig.2a, we can observe that pMSE increased as t increases for all models. SpaT-SparK showed the lowest pMSE among all models from t=1. This shows that SpaT-SparK is more accurate than others in the 1-hour period precipitation nowcasting. In Fig.2b, for accuracy, we can observe that SpaT-SparK outperforms SmaAt-UNet by a large margin and it has a moderate decrease as t increases. In Fig.2c and 2g,

we can observe that SparK underperforms SmaAt-UNet but our method outperforms SmaAt-UNet. This indicates that the translation network can help to improve precision and FAR performance. The improvements by the translation network can also be observed in Fig.2d to 2f and 2h for recall, F1, CSI, and HSS, respectively. This shows that the translation network is beneficial for encoder-decoder structured spatialtemporal model in precipitation nowcasting.

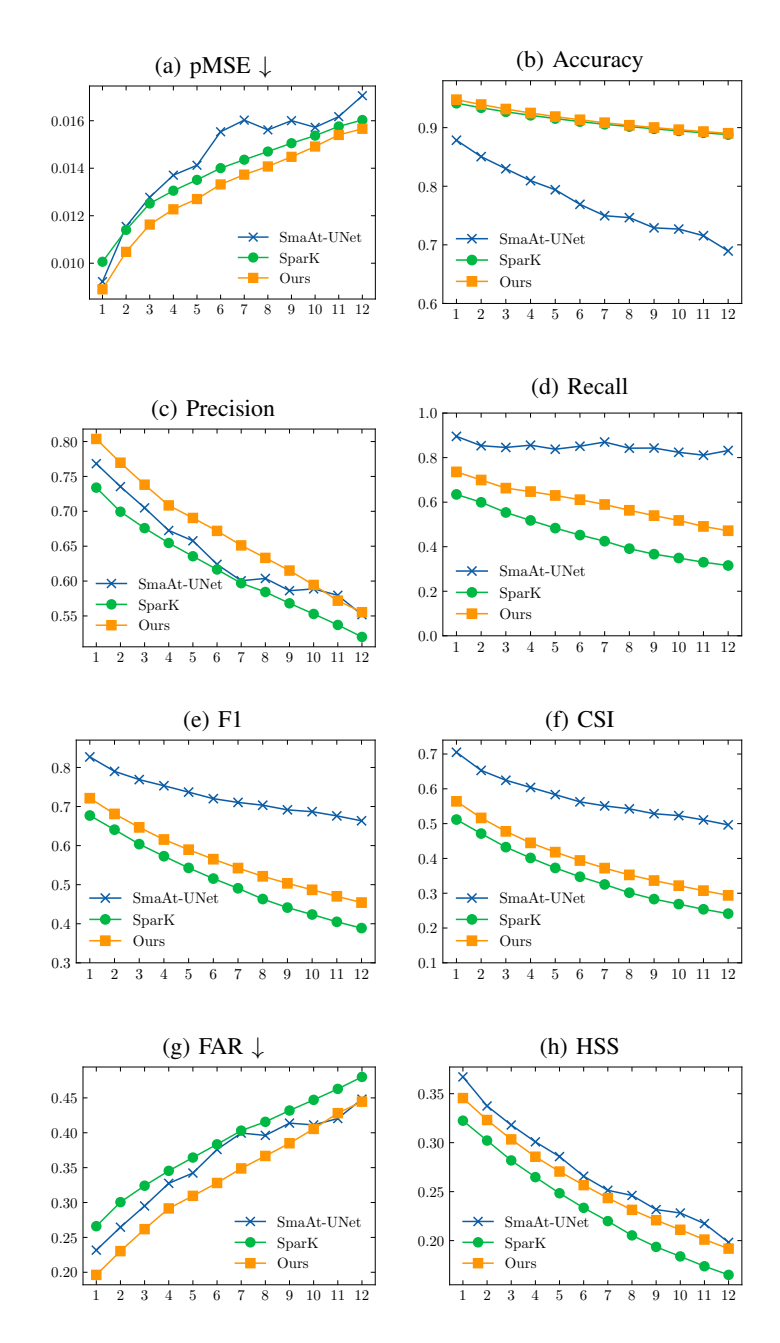


Fig. 2: Performance of the models at each time step. SparK and SpaT-SparK both use ResNet-18 as the encoder. "↓" indicates the lower the value is, the better the performance is.

Remark: While the results showed that SpaT-SparK out-

TABLE I: The performance comparison among SmaAt-UNet, SparK and SpaT-SparK with ResNet-18 or ResNet-50 as the encoder. "↑" indicates the higher the value is, the better the performance is. "↓" indicates the lower the value is, the better the performance is. The best result in each column is marked as bold.

Model	pMSE ↓	Accuracy ↑	Precision ↑	Recall ↑	F1 ↑	CSI ↑	FAR ↓	HSS ↑
SmaAt-UNet	0.0145	0.774	0.631	0.846	0.723	0.566	0.368	0.269
SparK								
ResNet-50	0.0136	0.911	0.646	0.520	0.543	0.373	0.353	0.245
ResNet-18	0.0139	0.910	0.620	0.444	0.512	0.344	0.379	0.232
SpaT-SparK								
ResNet-50	0.0135	0.911	0.633	0.486	0.528	0.359	0.366	0.239
ResNet-18	0.0132	0.913	0.678	0.588	0.560	0.389	0.321	0.255

TABLE II: Ablation study results. "↑" indicates the higher the value is, the better the performance is. "↓" indicates the lower the value is, the better the performance is. The best result in each column is marked as bold.

Method	pMSE ↓	Accuracy ↑	Precision ↑	Recall ↑	F1 ↑	CSI ↑	FAR ↓	HSS ↑
SpaT-SparK(ResNet18)	0.0132	0.913	0.678	0.588	0.560	0.389	0.321	0.255
w/o pretrain	0.0147	0.906	0.623	0.469	0.498	0.331	0.377	0.220
frozen-								
encoder	0.0140	0.912	0.687	0.602	0.545	0.375	0.313	0.246
decoder	0.0144	0.911	0.679	0.460	0.510	0.343	0.320	0.230
encoder+decoder	0.0147	0.909	0.642	0.444	0.495	0.329	0.358	0.221

performs baseline models in some numerical metrics, the visualizations of the predictions did not show sufficient quality improvements. This is probably the result of using a relatively large patch-size and the capability limitation of the decoder for generation.

Efficiency The inference time is another important factor for precipitation nowcasting applications. A method with shorter inference time and more accurate predictions are preferred. We measured the FLOPs, model size, and the model inference time for a single input on $1 \times$ NVIDIA A100 80GB GPU. The results are shown in Table III. We think that keeping the inference time in the magnitude of seconds makes it feasible as an application.

TABLE III: Efficiency performance. The data is measured on $1 \times NVIDIA A100 80GB GPU$.

Model	FLOPS(G)	#params(M)	pMSE
SmaAt-UNet	24.7	4.0	0.0145
SparK			
ResNet-18	99.2	43.4	0.0139
ResNet-50	110.8	53.0	0.0136
SpaT-SparK			
ResNet-18	172.6	96.5	0.0132
ResNet-50	184.1	106.0	0.0135

D. Ablation Study

We further investigate the effect of the pretraining and fine-tuning strategies. In Table II, we compare the model performance with an unpretrained encoder and/or decoder, a frozen encoder or decoder during fine-tuning, and summarize the results. The results showed that the complete SpaT-SparK model outperformed others in pMSE, accuracy, F1-score, CSI, and HSS. Without self-supervised pretraining, SpaT-SparK shows an obvious drop in all performance metrics. This necessitates the introduction of self-supervised pretraining again.

The frozen encoder during fine-tuning enabled the model to perform better than others in precision, recall and FAR, while only minor decreases are observed in accuracy, F1-score, and CSI. We also observed that SpaT-SparK model could achieve faster convergence to the best performance compared to those without pretraining, or partially/completely parameter freezing strategies. In conclusion, we think both the self-supervised pretraining and the translation network improved the performance of precipitation nowcasting.

VI. CONCLUSION AND FURTHER WORK

In this study, we proposed SpaT-SparK model to address this problem by leveraging the power of self-supervised learning and spatial-temporal modelling. We pretrained the encoder and the decoder in a self-supervised masked image modeling fashion. Then we employ a translation network to tackle the spatial-temporal transformation problem in fine-tuning. Our study reveals the potential of applying self-supervised learning in precipitation nowcasting. Future studies can focus on selecting optimal self-supervised learning strategy for learning representations of precipitation maps, and designing a more efficient translation network to capture capturing the dynamics of learned representations in the latent space.

REFERENCES

- Y. Wang, E. Coning, A. Harou, W. Jacobs, P. Joe, L. Nikitina, R. Roberts,
 J. Wang, J. Wilson, A. Atencia, B. Bica, B. Brown, S. Goodmann,
 A. Kann, P. W. Li, I. Monterio, F. Schmid, A. Seed, and J. Sun,
 Guidelines for Nowcasting Techniques, 11 2017.
- [2] R. O. Imhoff, C. C. Brauer, A. Overeem, A. H. Weerts, and R. Uijlenhoet, "Spatial and temporal evaluation of radar rainfall nowcasting techniques on 1,533 events," *Water Resources Research*, vol. 56, 2020.
- [3] P. Beça, A. C. Rodrigues, J. P. Nunes, P. Diogo, and B. Mujtaba, "Optimizing reservoir water management in a changing climate," *Water Resources Management*, pp. 1–15, 2023.
- [4] L. Foresti, M. Reyniers, A. Seed, and L. Delobbe, "Development and verification of a real-time stochastic precipitation nowcasting system for urban hydrology in belgium," *Hydrology and Earth System Sciences*, vol. 20, no. 1, pp. 505–527, 2016.

- [5] N. K. Johnson, Weather Prediction by Numerical Process. JSTOR, 1922.
- [6] K. A. Browning and C. G. Collier, "Nowcasting of precipitation systems," *Reviews of Geophysics*, vol. 27, no. 3, pp. 345–370, 1989.
- [7] J. Bech and J. L. Chau, Doppler radar observations: Weather radar, wind profiler, ionospheric radar, and other advanced applications. BoD–Books on Demand, 2012.
- [8] X. Shi, Z. Chen, H. Wang, D.-Y. Yeung, W.-K. Wong, and W.-c. Woo, "Convolutional lstm network: A machine learning approach for precipitation nowcasting," *Advances in neural information processing* systems, vol. 28, 2015.
- [9] S. Agrawal, L. Barrington, C. Bromberg, J. Burge, C. Gazen, and J. Hickey, "Machine learning for precipitation nowcasting from radar images," arXiv preprint arXiv:1912.12132, 2019.
- [10] K. Trebing, T. Stanczyk, and S. Mehrkanoon, "SmaAt-UNet: Precipitation now-casting using a small attention-unet architecture," *Pattern Recognition Letters*, vol. 145, pp. 178–186, May 2021.
- [11] S. Ravuri, K. Lenc, M. Willson, D. Kangin, R. Lam, P. Mirowski, M. Fitzsimons, M. Athanassiadou, S. Kashem, S. Madge, R. Prudden, A. Mandhane, A. Clark, A. Brock, K. Simonyan, R. Hadsell, N. Robinson, E. Clancy, A. Arribas, and S. Mohamed, "Skillful precipitation nowcasting using deep generative models of radar," *Nature*, vol. 597, no. 7878, pp. 672–677, Sep. 2021.
- [12] S. Mehrkanoon, "Deep shared representation learning for weather elements forecasting," *Knowledge-Based Systems*, vol. 179, pp. 120–128, 2019.
- [13] K. Trebing and S. Mehrkanoon, "Wind speed prediction using multidimensional convolutional neural networks," in 2020 IEEE symposium series on computational intelligence (SSCI). IEEE, 2020, pp. 713–720.
- [14] A. Kolesnikov, X. Zhai, and L. Beyer, "Revisiting self-supervised visual representation learning," in *Proceedings of the IEEE/CVF conference on* computer vision and pattern recognition, 2019, pp. 1920–1929.
- [15] H. Banville, O. Chehab, A. Hyvärinen, D.-A. Engemann, and A. Gramfort, "Uncovering the structure of clinical eeg signals with self-supervised learning," *Journal of Neural Engineering*, vol. 18, no. 4, p. 046020, 2021.
- [16] S. Kazatzidis and S. Mehrkanoon, "A novel dual-stream time-frequency contrastive pretext tasks framework for sleep stage classification," in 2024 International Joint Conference on Neural Networks (IJCNN). IEEE, 2024, pp. 1–8.
- [17] A. Elnaggar, M. Heinzinger, C. Dallago, G. Rehawi, Y. Wang, L. Jones, T. Gibbs, T. Feher, C. Angerer, M. Steinegger et al., "Prottrans: Toward understanding the language of life through self-supervised learning," *IEEE transactions on pattern analysis and machine intelligence*, vol. 44, no. 10, pp. 7112–7127, 2021.
- [18] T. Chen, S. Kornblith, K. Swersky, M. Norouzi, and G. E. Hinton, "Big self-supervised models are strong semi-supervised learners," *Advances in neural information processing systems*, vol. 33, pp. 22243–22255, 2020.
- [19] D. Hendrycks, M. Mazeika, S. Kadavath, and D. Song, "Using self-supervised learning can improve model robustness and uncertainty," Advances in neural information processing systems, vol. 32, 2019.
- [20] D. Pathak, P. Krahenbuhl, J. Donahue, T. Darrell, and A. A. Efros, "Context encoders: Feature learning by inpainting," in *Proceedings of the IEEE conference on computer vision and pattern recognition*, 2016, pp. 2536–2544.
- [21] K. He, X. Chen, S. Xie, Y. Li, P. Dollár, and R. Girshick, "Masked autoencoders are scalable vision learners," in *Proceedings of the IEEE/CVF conference on computer vision and pattern recognition*, 2022, pp. 16 000–16 009.
- [22] A. Gupta, J. Wu, J. Deng, and F.-F. Li, "Siamese masked autoen-coders," Advances in Neural Information Processing Systems, vol. 36, pp. 40 676–40 693, 2023.
- [23] R. Bachmann, D. Mizrahi, A. Atanov, and A. Zamir, "Multimae: Multimodal multi-task masked autoencoders," in *European Conference on Computer Vision*. Springer, 2022, pp. 348–367.
- [24] K. Tian, Y. Jiang, Q. Diao, C. Lin, L. Wang, and Z. Yuan, "Designing bert for convolutional networks: Sparse and hierarchical masked modeling," arXiv:2301.03580, 2023.
- [25] O. Ronneberger, P. Fischer, and T. Brox, "U-net: Convolutional networks for biomedical image segmentation," in *International Conference on Medical image computing and computer-assisted intervention*. Springer, 2015, pp. 234–241.

- [26] Y. Yang and S. Mehrkanoon, "AA-TransUnet: Attention augmented transunet for nowcasting tasks," in *International Joint Conference on Neural Networks (IJCNN)*. IEEE, 2022, pp. 01–08.
- [27] M. Renault and S. Mehrkanoon, "SAR-UNet: Small attention residual unet for explainable nowcasting tasks," in *International Joint Conference* on Neural Networks (IJCNN). IEEE, 2023, pp. 1–8.
- [28] J. G. Fernández and S. Mehrkanoon, "Broad-UNet: Multi-scale feature learning for nowcasting tasks," *Neural Networks*, vol. 144, pp. 419–427, 2021.
- [29] F. Chollet, "Xception: Deep learning with depthwise separable convolutions," in *Proceedings of the IEEE conference on computer vision and* pattern recognition, 2017, pp. 1251–1258.
- [30] S. Woo, J. Park, J.-Y. Lee, and I. S. Kweon, "Cbam: Convolutional block attention module," in *Proceedings of the European conference on* computer vision (ECCV), 2018, pp. 3–19.
- [31] E. Reulen, J. Shi, and S. Mehrkanoon, "GA-SmaAt-GNET: Generative adversarial small attention gnet for extreme precipitation nowcasting," *Knowledge-Based Systems*, vol. 305, p. 112612, 2024.
- [32] L. Vatamány and S. Mehrkanoon, "Graph dual-stream convolutional attention fusion for precipitation nowcasting," *Engineering Applications* of Artificial Intelligence, vol. 141, p. 109788, 2025.
- [33] R. Lam, A. Sanchez-Gonzalez, M. Willson, P. Wirnsberger, M. Fortunato, F. Alet, S. Ravuri, T. Ewalds, Z. Eaton-Rosen, W. Hu et al., "Learning skillful medium-range global weather forecasting," Science, vol. 382, no. 6677, pp. 1416–1421, 2023.
- [34] K. Bi, L. Xie, H. Zhang, X. Chen, X. Gu, and Q. Tian, "Accurate medium-range global weather forecasting with 3d neural networks," *Nature*, vol. 619, no. 7970, pp. 533–538, 2023.
- [35] T. Kurth, S. Subramanian, P. Harrington, J. Pathak, M. Mardani, D. Hall, A. Miele, K. Kashinath, and A. Anandkumar, "Fourcastnet: Accelerating global high-resolution weather forecasting using adaptive fourier neural operators," in *Proceedings of the platform for advanced scientific com*puting conference, 2023, pp. 1–11.
- [36] X. Liu, F. Zhang, Z. Hou, Z. Wang, L. Mian, J. Zhang, and J. Tang, "Self-supervised Learning: Generative or Contrastive," *IEEE Transactions on Knowledge and Data Engineering*, pp. 1–1, 2021, arXiv:2006.08218 [cs, stat]. [Online]. Available: http://arxiv.org/abs/2006.08218
- [37] J. Gui, T. Chen, J. Zhang, Q. Cao, Z. Sun, H. Luo, and D. Tao, "A survey on self-supervised learning: Algorithms, applications, and future trends," arXiv preprint arXiv:2301.05712, 2023.
- [38] J. Devlin, M.-W. Chang, K. Lee, and K. Toutanova, "Bert: Pre-training of deep bidirectional transformers for language understanding," arXiv preprint arXiv:1810.04805, Oct 2018.
- [39] Y. Liu, M. Ott, N. Goyal, J. Du, M. Joshi, D. Chen, O. Levy, M. Lewis, L. Zettlemoyer, and V. Stoyanov, "Roberta: A robustly optimized bert pretraining approach," arXiv preprint arXiv:1907.11692, 2019.
- [40] A. Dosovitskiy, L. Beyer, A. Kolesnikov, D. Weissenborn, X. Zhai, T. Unterthiner, M. Dehghani, M. Minderer, G. Heigold, S. Gelly et al., "An image is worth 16x16 words: Transformers for image recognition at scale," arXiv preprint arXiv:2010.11929, 2020.
- [41] X. Man, C. Zhang, C. Li, and J. Shao, "W-mae: Pre-trained weather model with masked autoencoder for multi-variable weather forecasting," arXiv preprint arXiv:2304.08754, Apr 2023.
- [42] H. Hersbach, B. Bell, P. Berrisford, S. Hirahara, A. Horányi, J. Muñoz-Sabater, J. Nicolas, C. Peubey, R. Radu, D. Schepers et al., "The era5 global reanalysis," *Quarterly Journal of the Royal Meteorological Society*, vol. 146, no. 730, pp. 1999–2049, 2020.
- [43] C. Tan, Z. Gao, S. Li, and S. Z. Li, "Simvp: Towards simple yet powerful spatiotemporal predictive learning," arXiv preprint arXiv:2211.12509, 2022.
- [44] C. Tan, S. Li, Z. Gao, W. Guan, Z. Wang, Z. Liu, L. Wu, and S. Z. Li, "Openstl: A comprehensive benchmark of spatio-temporal predictive learning," *Advances in Neural Information Processing Systems*, vol. 36, pp. 69819–69831, 2023.
- [45] C. Wei, H. Fan, S. Xie, C.-Y. Wu, A. Yuille, and C. Feichtenhofer, "Masked feature prediction for self-supervised visual pre-training," 2023. [Online]. Available: https://arxiv.org/abs/2112.09133
- [46] K. He, X. Zhang, S. Ren, and J. Sun, "Deep residual learning for image recognition," in *Proceedings of the IEEE conference on computer vision* and pattern recognition, 2016, pp. 770–778.
- [47] Y. You, J. Li, S. Reddi, J. Hseu, S. Kumar, S. Bhojanapalli, X. Song, J. Demmel, K. Keutzer, and C.-J. Hsieh, "Large batch optimization for deep learning: Training bert in 76 minutes," arXiv preprint arXiv:1904.00962, 2019.